J. Fluid Mech. (1989), *vol.* 201, *pp.* 77–97
Printed in Great Britain

Three-dimensional wave packets and instability waves in free shear layers and their receptivity

By THOMAS F. BALSA

Department of Aerospace and Mechanical Engineering, University of Arizona, Tucson, AZ 85721, USA

(Received 16 December 1987 and in revised form 30 August 1988)

In this paper, we study the evolution of strongly three-dimensional disturbances which are generated by a point force in a parallel mixing layer. When the input force is a pulse, a wave packet develops whose wavefronts are approximately parallel to the spanwise direction. This is in sharp contrast to a wave packet in a wall boundary layer for which the wavefronts are strongly curved. On the other hand, when the input disturbance is oscillating harmonically in time, a spatially growing instability wave develops in a downstream wedge of (x, z)-space. The size of this wedge, as a function of excitation frequency and velocity ratio, is determined. The receptivity of the shear layer to pulse-type and harmonic excitation is also studied. It is found that the shear layer is especially sensitive to relatively high-frequency forcing on its centreline.

1. Introduction

It is now generally recognized that large-scale or coherent structures play an important role in the dynamics of turbulent free shear flows. These structures have their origin in the instability modes of the 'fictitious' time-averaged mean flow. There is mounting experimental evidence which suggests that these larger scales of the flow can be organized by low-level periodic forcing – in this case the large-scale motions become quasi-deterministic and describable by the methods of linear and nonlinear stability analyses for slowly diverging base flows (Crighton & Gaster 1976; Gaster, Kit & Wygnanski 1985; Goldstein & Leib 1988).

For this reason, there is a renewed interest in the stability analysis of various types of shear flows. Whereas in classical stability theory the principal objective is the determination of the temporal stability of the flow via modal analysis (Betchov & Criminale 1967; Drazin & Reid 1981), recent stability studies focus on spatial modes and spatio-temporal modes (Monkewitz & Nguyen 1987). The former describe the spatial evolution of infinitely long wavetrains while the latter characterize the corresponding behaviour of finite-length wavetrains (i.e. wave packets). The condition under which two-dimensional spatial instability modes actually evolve in a harmonically excited free shear layer has been discussed by Huerre & Monkewitz (1985). The precise requirement is that the flow be *convectively* unstable and, roughly speaking, this implies that the velocity of the reverse flow (if any) be quite small.

It is well known that a wave packet, which is the response of a base flow to a spatially compact pulse-type input disturbance, is the link between temporal and spatial instability modes (Criminale & Kovasznay 1962; Gaster 1968). This link can be made extremely strong and precise by synthesizing a spatial mode from a series of wave packets (Balsa 1988); this is the approach that we shall follow in the present

paper in our discussion of highly three-dimensional spatial instability modes generated by point forces. However, wave packets are physically interesting entities in their own right since they appear to break down to turbulence at lower amplitudes than infinite wave trains (Gaster 1981). In fact, it is reasonable to think of a turbulent spot as a highly aged wave packet. Gaster attributes this earlier breakdown in the wall boundary layer to the form of the Reynolds stress that will be dominated, in the case of the packet, by large amplitude modulations. Therefore, we begin our discussion with three-dimensional wave packets in shear layers and compare their characteristics with those in a wall boundary layer.

This is done by solving the initial-value problem and by studying its long-time behaviour (§3). The entire problem is formulated in §2. Our approach is partly classical in the sense that the streamwise and spanwise coordinates are extracted by Fourier transforms but the remaining partial differential equations (in the transverse coordinate, y, and time, t) are solved directly (without the use of a Laplace transform in time). In this respect, as well as on some other essential points such as the presence of interfaces and the three-dimensionality of the flow, the present approach differs from the work of Case (1960, 1961). The main message is that a Laplace transform in time is not really needed, and we shall omit it for simplicity at the outset. As seen from (10a, b), our solution consists of two Rayleigh modes (an unstable/stable pair) and a 'convected mode' (essentially the continuum mode of Case). The continuum mode arises because the vorticity, which is placed in the flow initially, must be convected (and possibly stretched) by the flow. From physical considerations, it is clear that the basic instability of a shear layer has nothing to do with this 'passive' convection of the initial vorticity, so that the continuum modes do not play an important role in the large-time asymptotic solution which is determined by the unstable discrete modes.

The main significance of the solution to the inital-value problem is that it tells us the extent to which a discrete instability mode is excited by the given initial disturbance. In other words, the solution of the initial-value problem determines the *receptivity* of the flow; that is, it determines the amplitude of each mode. Although some theoretical work has been done on the receptivity of wall boundary layers (Goldstein 1983), no results exist for free shear flows. We believe that the results of this paper are quite representative of the behaviour of the flow field generated by compact disturbances in shear layers (e.g. small heating elements or tiny jets).

In §§4 and 5, we describe the highly three-dimensional instability wave (and the corresponding receptivity) which is produced by a harmonically oscillating point force. Perhaps the most interesting geometric feature of this problem is the presence of a 'wedge of influence' in (x, z)-space. This wedge contains all the instability waves generated by the force and is reminiscent of the Mach wedge in supersonic flows. We also discuss the geometry of this wedge as a function of the similarity parameters of the problem.

In summary, the contributions of this paper are: a comparison of wave packets in a wall boundary and free shear layers, the receptivity of a shear layer to spatially compact pulse-type and periodic excitation, and the elucidation of the downstream structure of the instability wave which is shed behind an oscillating point force.

2. Formulation of the problem and its solution

Consider a unidirectional parallel shear flow whose velocity components are [$U(y)$, 0, 0], where $\boldsymbol{x} = (x, y, z,)$ is a right-handed Cartesian coordinate system. Let this base

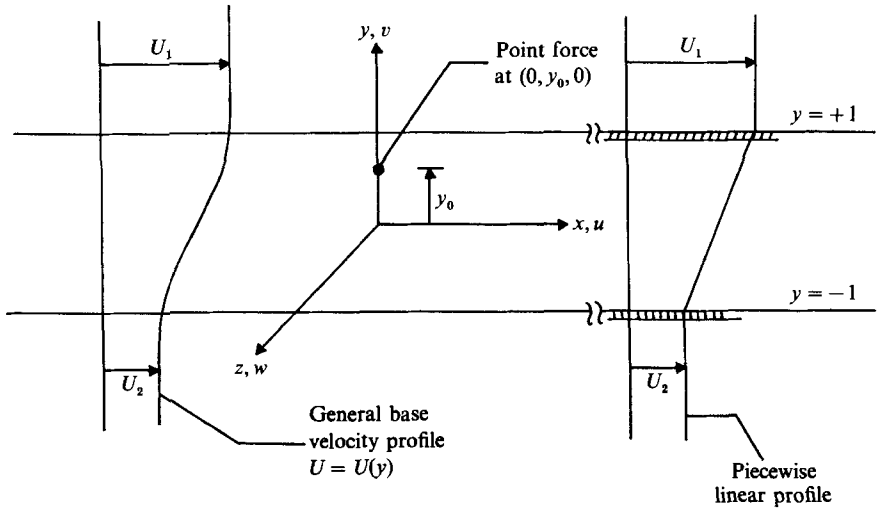

FIGURE 1. Geometry of the problem.

flow be perturbed by a volume force $\boldsymbol{F}$ whose components are $F_x = F_z = 0$ and $F_y = -\epsilon\delta(x)\,\delta(y-y_0)\,\delta(z)\,\delta(t)$, where $\delta(\xi)$ is the delta function with support at $\xi = 0$. The y-component of the total impulse exerted on the fluid is $(-\epsilon)$. This spatially compact force is located at the point $(0,\ y_0,\ 0)$, where y_0 denotes the transverse coordinate of the force (figure 1). The force acts on the fluid only for a brief instant of time (t = time). One of our objectives is to study the spatial and temporal characteristics of the disturbance generated by this force using linear theory.

Under the assumption that the flow is incompressible with unit density, the governing equations are

$$\nabla\cdot\boldsymbol{u} = 0, \tag{1a}$$

$$\frac{\mathrm{D}\boldsymbol{u}}{\mathrm{D}t} + v\frac{\mathrm{d}U}{\mathrm{d}y}\boldsymbol{i} = -\nabla p + F_y\boldsymbol{j}, \tag{1b}$$

where the perturbation velocity is denoted by $\boldsymbol{u} = (u,\ v,\ w)$, p is the perturbation pressure, and $\boldsymbol{i}$, $\boldsymbol{j}$ are the unit vectors in the x- and y-directions, respectively. $\mathrm{D}/\mathrm{D}t = \partial/\partial t + U\partial/\partial x$ is the convective derivative following the base flow.

We may think of the solution $(\boldsymbol{u}, p)$ as the fundamental solution or Green function. This, together with the principle of superposition, can be used to describe the response of the shear layer to any y-force. Although the techniques of the present paper may be applied to investigate the effects of the other two components of the force, we restrict our attention to a y-force only in the present analysis; from an experimental point of view, a shear layer is usually perturbed by a 'transverse disturbance' (such as an oscillating trailing edge flap or a vibrating ribbon).

Our governing equations $(1a, b)$ are solved with specific initial conditions which state that prior to the impulsive triggering of the flow by the force, all perturbations are null

$$\boldsymbol{u} = p = 0 \quad \text{for } t < 0. \tag{2}$$

Furthermore, at large distances, $(x^2+y^2+z^2)^{\frac{1}{2}} \to \infty$, all disturbances are required to vanish. We are interested in the complete solution to the initial-value problem, not merely the growth rate, phase velocity, or shape of a specified mode. This is because we wish to study the response of the flow to our specific excitation. In other words,

we wish to study how a 'transverse disturbance' excites the instability modes of a shear layer and the relationship between these modes and the excitation which produces them. We call this relationship the receptivity of the shear layer.

We shall solve (1 *a*, *b*) by the use of Fourier transforms in the x- and z-directions. A Laplace transform in time is avoided altogether for the sake of simplicity. Introduce the Fourier transform pairs by

$$(\hat{\cdot}) = \frac{1}{2\pi}\int_{-\infty}^{\infty}\int_{-\infty}^{\infty}(\cdot)\mathrm{e}^{-\mathrm{i}(kx+lz)}\,\mathrm{d}x\,\mathrm{d}z, \tag{3a}$$

$$(\cdot) = \frac{1}{2\pi}\int_{-\infty}^{\infty}\int_{-\infty}^{\infty}(\hat{\cdot})\mathrm{e}^{+\mathrm{i}(kx+lz)}\,\mathrm{d}k\,\mathrm{d}l, \tag{3b}$$

where k and l are the wavenumbers in the streamwise and spanwise directions, respectively. After transforming (1 *a*, *b*) and performing some straightforward algebra to eliminate all variables in favour of $\hat{v}$, we arrive at

$$\left(\frac{\partial}{\partial t}+\mathrm{i}kU\right)\left(\frac{\partial^2\hat{v}}{\partial y^2}-\kappa^2\hat{v}\right)-\mathrm{i}k\hat{v}\frac{\mathrm{d}^2U}{\mathrm{d}y^2} = -\kappa^2\hat{F}_y, \tag{4}$$

where $\kappa^2 = (k^2+l^2)$.

We may readily convert (4) into an integro-differential equation by finding the inverse of the convective operator $(\partial/\partial t+\mathrm{i}kU)$. This results in

$$\frac{\partial^2\hat{v}}{\partial y^2}-\kappa^2\hat{v} = \mathrm{i}kU''\mathrm{e}^{-\mathrm{i}kUt}\int_{0^-}^{t}\hat{v}(\tau)\,e^{+\mathrm{i}kU\tau}\,\mathrm{d}\tau+\frac{\kappa^2}{2\pi}\delta(y-y_0)\,\mathrm{e}^{-\mathrm{i}kU_0t}\,H(t), \tag{5}$$

where the primes denote differentiation with respect to y, $U_0 = U(y_0)$, $H(t)$ is the Heaviside function, and we have written $\hat{v}(\tau)$ for $\hat{v}(k, y, l, \tau)$. Note that in obtaining (5) we have enforced the inital condition $\hat{v} = 0$ at $t = 0^-$ and set the strength of the impulse, ϵ, to unity since our problem is linear in ϵ. Observe also that there is no loss in generality by choosing two of the coordinates of the point force to be $x = 0$ and $z = 0$ since the base flow is homogeneous in these directions.

Since our primary interest is in the receptivity of shear layers and in the qualitative description of the evolution of three-dimensional disturbances, we will assume that the base velocity $U = U(y)$ is given by the piecewise linear profile of Rayleigh

$$U(y) = \begin{cases} U_1 = \text{const} & (y \geqslant 1), \\ U_m+\frac{1}{2}\Delta U y & (|y| \leqslant 1), \\ U_2 = \text{const} & y \leqslant -1), \end{cases} \tag{6}$$

where $U_m = \frac{1}{2}(U_1+U_2)$ and $\Delta U = U_1-U_2$. Both the temporal and spatial instability characteristics of this profile approximate very closely the large Reynolds number instabilities of a class of infinitely smooth profiles which differ from (6) only in two very narrow regions at the edges of the layer, say $y = \pm 1$ (figure 1). A more detailed justification of these remarks is given elsewhere (Balsa 1987). The simplicity and usefulness of the Rayleigh profile is unquestionable, and it is sufficient to note here that for this profile, we can solve the initial-value problem in closed form, hence the structure of the solution and the evolution of the modes become completely transparent and are not hidden in excessive numerical calculations (Balsa 1988). Some of our procedures are applicable to general parallel flows, and the results

obtained herein apply qualitatively to these flows. It is also worth pointing out that the evolution of wavelike disturbances (linear and nonlinear) in unbounded shear flows, with spatially uniform shear rates, has been studied by Lagnado, Phan-Thien & Leal (1984), Bayly (1986), and Craik & Criminale (1986) in a very general setting.

Our integro-differential equation (5) assumes an extremely simple form for the piecewise linear profile since $U'' \equiv 0$ (except at $y = \pm 1$, where we use interface matching conditions). We find, for $t > 0$,

$$\frac{\partial^2 \hat{v}}{\partial y^2} - \kappa^2 \hat{v} = \chi(k, \kappa, t)\,\delta(y - y_0), \tag{7a}$$

where

$$\chi(k, \kappa, t) = \frac{\kappa^2}{2\pi} e^{-ikU_0 t}. \tag{7b}$$

The principal task ahead of us is to solve (7*a*) with decaying boundary conditions at $|y| \to \infty$ such that $\hat{v}$ and $\hat{p}$ are continuous across the shear layer interfaces at $y = \pm 1$. We first concentrate on the case when the force is located within the shear layer; $|y_0| \leqslant 1$.

For this case there are four regions of interest and, in each of these, the solution for $\hat{v}$ may be written as a linear combination of $\exp(\pm \kappa y)$, where $\kappa = (k^2 + l^2)^{\frac{1}{2}}$ such that $\mathrm{Re}\,(\kappa) \geqslant 0$, where $\mathrm{Re}\,(\cdot)$ denotes the real part of a complex number. Note that, in general, we must permit the streamwise and spanwise wavenumbers (k, l) to be complex and the inversion of the Fourier transform (3*b*) is taken along suitably chosen contours in the complex k- and l-planes.

By elementary considerations, we have

$$\hat{v} = \begin{cases} A\, e^{-\kappa(y-1)} & (y \geqslant 1), \\ A\cosh[\kappa(y-1)] + C\sinh[\kappa(y-1)] & (y_0 < y \leqslant 1), \\ B\cosh[\kappa(y+1)] + E\sinh[\kappa(y+1)] & (-1 \leqslant y < y_0), \\ B\, e^{+\kappa(y+1)} & (y \leqslant -1), \end{cases} \tag{8}$$

where (8) already satisfies the decaying boundary conditions at $|y| \to \infty$ and the continuity of $\hat{v}$ across the interfaces. Note that A, B, C and E are coefficients depending on time (but not on y).

We shall use $A = A(t)$ and $B = B(t)$ as our principal variables since $C(t)$ and $E(t)$ can be readily expressed in terms of the former. This is accomplished by enforcing the usual matching conditions across the force location $y = y_0$. The final result is

$$\left.\begin{matrix} C \\ E \end{matrix}\right\} \sinh 2\kappa = \left.\begin{matrix} +A \\ -B \end{matrix}\right\} \cosh 2\kappa \left.\begin{matrix} -B \\ +A \end{matrix}\right\} + \frac{\chi(k, \kappa, t)}{\kappa} \sinh[\kappa(y_0 \pm 1)]. \tag{9}$$

The equations for $A(t)$ and $B(t)$ come from the requirement that the Fourier transform of the pressure is continuous across the interfaces. This requirement can be readily satisfied by using the linearized x-component of the momentum equations. After some straightforward algebra we arrive at the coefficients in (8):

$$\begin{aligned} \tilde{A}(t) = {} & e^{\lambda\tau}\{[A(0^+) - a](\lambda + ia_{11}) + ia_{12}[B(0^+) - b]\}/2\lambda \\ & + e^{-\lambda\tau}\{-ia_{12}[B(0^+) - b] + [A(0^+) - a](\lambda - ia_{11})\}/2\lambda + a\exp[-ik(U_0 - U_m)t], \end{aligned} \tag{10a}$$

$$\tilde{B}(t) = \mathrm{e}^{\lambda\tau}\left\{[A(0^+)-a]\frac{(\lambda-\mathrm{i}a_{11})(\lambda+\mathrm{i}a_{11})}{\mathrm{i}a_{12}}+[B(0^+)-b](\lambda-\mathrm{i}a_{11})\right\}\Big/2\lambda$$
$$+\mathrm{e}^{-\lambda\tau}\left\{-[A(0^+)-a]\frac{(\lambda-\mathrm{i}a_{11})(\lambda+\mathrm{i}a_{11})}{\mathrm{i}a_{12}}+[B(0^+)-b](\lambda+\mathrm{i}a_{11})\right\}\Big/2\lambda$$
$$+b\exp[-\mathrm{i}k(U_0-U_m)t], \quad (10b)$$

where, in (10a, b), the quantities a, λ, etc., are evaluated at κ (i.e. $a = a(\kappa)$, etc.) and $\tau = \Delta U t k/\kappa$. Note that $(\tilde{\cdot}) = (\cdot)\exp(+\mathrm{i}kU_m t)$, $U_m = \frac{1}{2}(U_1+U_2)$, and $\Delta U = U_1-U_2$.

Furthermore, in deriving the last set of equations, we have used the following definitions:

$$\left.\begin{aligned}A(0^+) &= \tilde{A}(0^+)\\ B(0^+) &= \tilde{B}(0^+)\end{aligned}\right\} = -\frac{\chi(k,\kappa,0)}{2\kappa}\mathrm{e}^{-\kappa}\mathrm{e}^{\pm\kappa y_0}, \quad (11)$$

$$\lambda(\kappa) = \tfrac{1}{4}\{\mathrm{e}^{-4\kappa}-(1-2\kappa)^2\}^{\frac{1}{2}}, \quad (12a)$$

$$\mathscr{D}(\kappa) = (\tfrac{1}{2}\kappa y_0)^2+\lambda^2(\kappa), \quad (12b)$$

$$\left.\begin{aligned}a(\kappa)\\ b(\kappa)\end{aligned}\right\} = \tfrac{1}{4}\chi(k,\kappa,0)(y_0\mp 1)\{\sinh[\kappa(y_0\pm 1)][\tfrac{1}{2}\mathrm{e}^{-2\kappa}\mp(y_0\pm 1)\Gamma(\kappa)]$$
$$\pm(y_0\pm 1)\Gamma(\kappa)\mathrm{e}^{-2\kappa}\sinh[\kappa(y_0\mp 1)]\}/\mathscr{D}(\kappa) \quad (13)$$

$$a_{11} = a_{11}(\kappa) = \tfrac{1}{4}-\Gamma\cosh 2\kappa \quad (14a)$$

$$a_{12} = a_{12}(\kappa) = \Gamma-\tfrac{1}{4}\mathrm{e}^{-2\kappa} \quad (14b)$$

and $\Gamma = \Gamma(\kappa) = \kappa/(2\sinh 2\kappa)$.

When the force is located outside the shear layer (i.e. $|y_0| \geqslant 1$), we have the somewhat simpler result $a = b = 0$ and

$$\left.\begin{aligned}A(0^+) &= \tilde{A}(0^+)\\ B(0^+) &= \tilde{B}(0^+)\end{aligned}\right\} = -\frac{\chi(k,\kappa,0}{2\kappa}\mathrm{e}^{-\kappa|y_0|}\exp[\pm\kappa\,\mathrm{sgn}\,(y_0)], \quad (15)$$

where $\mathrm{sgn}\,(y_0) = \pm 1$ according to $y_0 > 0$ or $y_0 < 0$. Otherwise, (10a, b) hold for $\tilde{A}(t)$ and $\tilde{B}(t)$.

In order to keep our results manageable, we shall focus on the transverse velocity component at the upper interface. Similar results may be obtained for other quantities of physical interest. From (8), (3b), and the definition of $\tilde{A}$, we find

$$v(x,\,1,\,z,\,t) = \frac{1}{2\pi}\int_{-\infty}^{\infty}\int_{-\infty}^{\infty}\tilde{A}(t)\exp[\mathrm{i}k(x-U_m t)+\mathrm{i}lz]\,\mathrm{d}k\,\mathrm{d}l. \quad (16)$$

Under the assumption that $\Delta U = U_1-U_2 > 0$, the most important contribution to (16), for large times, comes from the first term of $\tilde{A}(t)$ – this term corresponds to the unstable mode of the shear layer. The precise mathematical arguments for the validity of the last remark were given by Balsa (1988) and will not be repeated here. Physically, however, it is plausible that the large-time solution should be dominated by the unstable mode. For these reasons, (16) may be rewritten as

$$v(x,\,1,\,z,\,t) = \frac{1}{2\pi}\int_{-\infty}^{\infty}\int_{-\infty}^{\infty}\exp[\mathrm{i}k(x-U_m t)+\mathrm{i}lz]\,\mathrm{e}^{\lambda(\kappa)\tau}\mathscr{F}_1(\kappa)\,\mathrm{d}k\,\mathrm{d}l, \quad (17a)$$

for $t \to \infty$, where

$$\mathscr{F}_1(\kappa) = \{[A(0^+)-a](\lambda + ia_{11}) + ia_{12}[B(0^+)-b]\}/2\lambda. \tag{17b}$$

It is understood that the quantities $A(0^+)$, a, etc., appearing on the right-hand side of (17*b*), are evaluated at the argument κ as given by (12), (13), etc. Note that in (12*a*), we choose the principal square root such that $Z^{\frac{1}{2}}$ maps the complex Z-plane cut along the negative real axis onto the half space $\mathrm{Re}\,(Z^{\frac{1}{2}}) > 0$.

Note that our solution for $(\boldsymbol{u}, p)$ consists of an unstable/stable pair of Rayleigh modes corresponding to the first two terms of (10) and a 'convected' (i.e. continuum) mode corresponding to the last term of (10). There are no Squire modes in the present problem (because the flow is inviscid), and had we used a Laplace transform in time, the appearance of the Rayleigh and the continuum modes would have been slightly less transparent. However, from (4) and (5) it is seen that the origin of the exponential time factors in (5) is due to the 'removal' of the convective operator, $(\partial/\partial t + ikU)$, from (4). This is entirely equivalent to the inclusion of the continuum modes (Case 1960).

There remains to evaluate (17*a*) by the saddle point method in order to obtain a simple result for the velocity perturbations. This leads to the concept of a wave packet, which is described in the next section.

3. The three-dimensional wave packet

The fluid is perturbed by a point force located at $\boldsymbol{x} = (0, y_0, 0)$. This force acts on the shear layer for a brief instant of time, thereby disturbing the equilibrium state of the fluid represented by the parallel base flow. For large values of time, the many instability modes that were excited by the initial disturbance interfere with each other and produce a relatively simple structure, which is called a wave packet (Gaster 1968, 1975).

The form of this wave packet may be calculated by evaluating (17*a*) as $t \to \infty$ by the saddle point method. Since $\mathscr{F}_1$ depends only on the oblique wavenumber $\kappa = (k^2 + l^2)^{\frac{1}{2}}$, it is convenient to introduce polar coordinates (κ, θ) such that

$$k = \kappa \cos\theta, \tag{18a}$$

$$l = \kappa \sin\theta. \tag{18b}$$

As long as (k, l) are real, we may think of θ as the direction in (x, z)-space along which the wavefront of a three-dimensional oblique instability mode is propagating. (x, z) is called the propagation space (Hayes 1970)

In order to observe the detailed structure of the packet, we must move with the disturbance in some sense. Define moving observer velocity components $G = x/t$ and $L = z/t$ and represent these in terms of polar coordinates $(\mathscr{V}, \alpha)$ via

$$G - U_m = \mathscr{V} \cos\alpha, \tag{19a}$$

$$L = \mathscr{V} \sin\alpha \tag{19b}$$

where, of course, $\mathscr{V}$ and α are always real. Actually, (G, L) is the group velocity in propagation space, but we need not be concerned about this at this time.

Based on these opening remarks, (17*a*) can be rewritten as

$$v(x, 1, z, t) = \frac{1}{2\pi}\int_0^{2\pi}\int_0^{\infty} \mathrm{e}^{Th}\,\mathscr{F}_1(\kappa)\,\kappa\,\mathrm{d}\kappa\,\mathrm{d}\theta, \tag{20a}$$

where $$T = \Delta U t, \tag{20b}$$

and $$h = h(\kappa, \theta; \mathscr{V}/\Delta U, \alpha) = \mathrm{i}\kappa \frac{\mathscr{V}}{\Delta U}\cos(\theta-\alpha) + \lambda(\kappa)\cos\theta. \tag{20c}$$

It is now possible to evaluate (20a) quite simply as $t \to \infty$ for fixed values of the observer velocities G and L. The saddle points, $\kappa = \kappa_0(\mathscr{V}/\Delta U, \alpha)$ and $\theta = \theta_0(\mathscr{V}/\Delta U, \alpha)$, are given by the simultaneous solution of $\partial h/\partial\kappa = \partial h/\partial\theta = 0$ (Dingle 1973, p. 209). The final result is

$$v(x, 1, z, t) = \frac{2|\mathscr{H}|}{T}\exp(Th_{0_R})\cos(Th_{0_I} + \gamma), \tag{21a}$$

where $T = \Delta U t$,

$$h_0 = h_0(\mathscr{V}/\Delta U, \alpha) = h(\kappa_0, \theta_0; \mathscr{V}/\Delta U, \alpha), \tag{21b}$$

and $$\mathscr{H} = |\mathscr{H}|\,\mathrm{e}^{\mathrm{i}\gamma} = \frac{\mathscr{F}_1(\kappa_0)\,\kappa_0}{\{h_{\kappa\kappa}h_{\theta\theta} - h_{\kappa\theta}^2\}^{\frac{1}{2}}}. \tag{21c}$$

Note that γ (real) is the phase of the complex number $\mathscr{H}$, $\Delta U = U_1 - U_2 > 0$, and the subscripts R and I denote the real and imaginary parts of a complex number. Double subscripted variables denote partial derivatives evaluated at the saddle point (e.g. $h_{\kappa\kappa} = \partial^2 h/\partial\kappa^2$ at $\kappa = \kappa_0$ and $\theta = \theta_0$).

The receptivity of the shear layer to pulse-type disturbances is contained entirely in the complex-valued function $\mathscr{F}_1(\kappa)$ (see (17b)) evaluated at the saddle point $\kappa = \kappa_0$. We shall study the behaviour of this function in §5. The term 'receptivity' is used in this paper with two different meanings to quantify the responsiveness of a shear layer to pulse-type and periodic excitations. We note that (21a, c) contain all the usual terms associated with the saddle-point method (i.e. exponential growth due to the instability, oscillations due to the wave-like character of the perturbed flow, and a 'decay' term due to the geometric spreading of the 'rays' in propagation space as described by $\{T[h_{\kappa\kappa}h_{\theta\theta} - h_{\kappa\theta}^2]^{\frac{1}{2}}\}^{-1}$). Each one of these terms is completely independent of the excitation; the only term that contains any information about the excitation is $\mathscr{F}_1$. Therefore, $\mathscr{F}_1$ is a (reasonable) measure of the receptivity of our shear layer to a pulse. The general structure of a wave packet (apart from the factor $\mathscr{F}_1$) was discovered by Gaster (1968) and Gaster & Davey (1968), although an approximate structure was obtained by Criminale & Kovasznay (1962).

We may think of equations (19) as a mapping from propagation space (x, z) onto ($\mathscr{V}/\Delta U$, α) space (i.e. essentially group velocity space) via the transformation

$$\frac{x/t - U_m}{\Delta U} = \frac{\mathscr{V}}{\Delta U}\cos\alpha, \tag{22a}$$

$$\frac{z}{\Delta U t} = \frac{\mathscr{V}}{\Delta U}\sin\alpha. \tag{22b}$$

Quite often it is far more convenient to describe certain aspects of the packet in ($\mathscr{V}/\Delta U$, α)-space rather in propagation space. The last remark certainly holds true for the growth rate, h_{0_R} and Doppler-shifted frequency (as seen by the moving observer), h_{0_I}.

The behaviour of these quantities, as functions of $\mathscr{V}/\Delta U$, is shown in figure 2 for parametric values of α. It is seen that the growth of the packet is maximum at $\mathscr{V}/\Delta U = 0$ (i.e. $x = U_m t, z = 0$). We shall call this point the centre of the packet. As we move away from this point in the downstream direction ($\mathscr{V}/\Delta U > 0$, $\alpha = 0$), the growth rate drops off monotonically until we reach the edge of the packet at

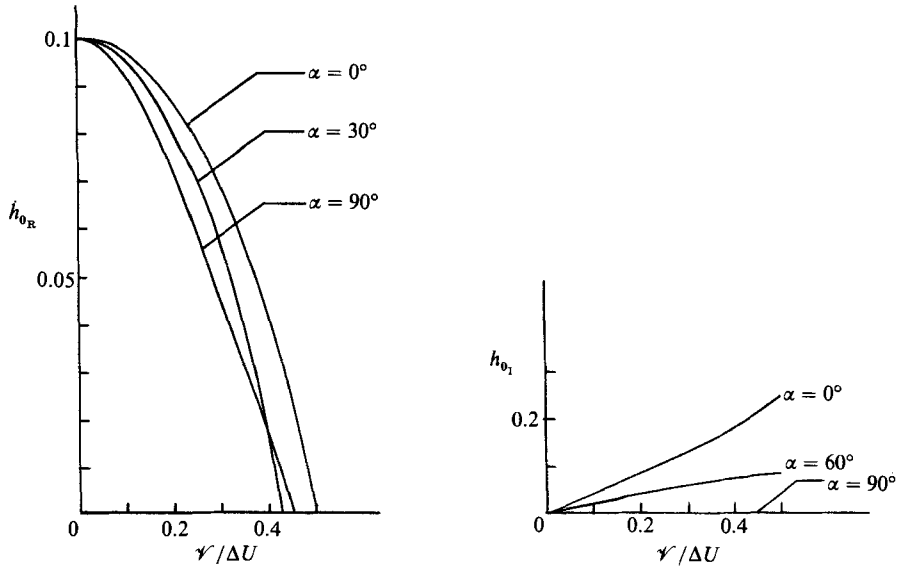

FIGURE 2. Wave packet growth rate (h_{0_R}) and Doppler-shifted frequency (h_{0_I}) as a function of group velocity ($\mathscr{V}/\Delta U$, α).

$\mathscr{V}/\Delta U = 0.5$ and $\alpha = 0$. Very similar remarks hold true for the other directions (i.e. for other values of α), although the edge of the packet depends somewhat on the precise value of α. Crudely speaking, we also see the central idea behind the Squire transformation in figure 2: oblique waves, with $\alpha \neq 0$, generally grow less rapidly than two-dimensional waves for which $\alpha = 0$. Indeed, the growth rate for $\alpha = 0$ is precisely the two-dimensional one (Balsa 1988). Note, however, that even 'cross-waves' ($\alpha = \frac{1}{2}\pi$) grow quite strongly. This conclusion points out the danger of applying the Squire transformation to modes with complex wavenumbers.

Clearly, there must be complete symmetry for h_{0_R} between the directions given by (α) and ($-\alpha$), as well as by (α) and ($\pi - \alpha$). In other words, there is left-to-right symmetry (facing downstream) as well as upstream and downstream symmetry, therefore, only results in the range $0 \leqslant \alpha \leqslant \frac{1}{2}\pi$ are shown.

The Doppler-shifted frequency, h_{0_I}, is very nearly a linear function of $\mathscr{V}/\Delta U$. This frequency is zero at the centre of the packet and increases monotonically as one moves in the downstream direction. In other words, one will see a wave-like pattern in the downstream direction as a result of a pulse-type excitation. On the other hand, in the spanwise direction ($\alpha = \frac{1}{2}\pi$) the frequency is identically zero for all values of $\mathscr{V}/\Delta U$. Therefore, there is no wave-like structure in this latter direction. Once again we have left-to-right symmetry, but antisymmetry in the upstream and downstream directions in the sense that the frequency h_{0_I} at $(\pi - \alpha)$ is the negative of h_{0_I} at α. It is absolutely essential to remember that these remarks on symmetry apply only to the growth rate and frequency and not to the disturbance velocity $v(x, 1, z, t)$. We shall discuss the symmetry properties of v in §5.

When a shear layer is perturbed by a pulse, at each instant of time, the exponentially large part of the disturbance will be contained (very roughly speaking) in a circular disk in (x, z)-space with the centre at $x = U_m t$, $z = 0$ and radius $\approx 0.5\,\Delta U t$. Clearly, in space (x, z, t), the zone of influence of this pulse will be a cone. This we shall call the *cone of influence*, whose geometry is shown in figure 3.

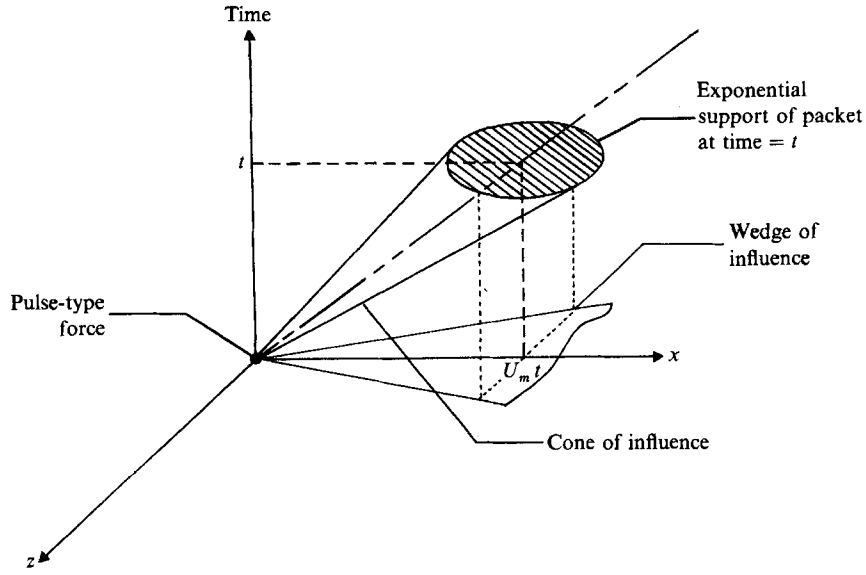

FIGURE 3. Cone of influence of a pulse-type point force in propagation space ($U_m > 0$).

The slenderness of the cone, which measures the rate at which the wave packet is spreading out in space, is given by $0.5\,\Delta U/U_m$ (approximately).

4. Periodic excitation by a point force

An oscillating point force in a shear layer will generate a complicated three-dimensional disturbance. Very little work has been done on three-dimensional disturbances, either theoretically or experimentally. In classical temporal stability theory, usually some form of the Squire transformation is invoked to assess the stability of the flow. On the other hand, very little is known about the spatial stability of three-dimensional disturbances in shear flows (Michalke 1969).

Our principal aim in this section is to synthesize the response of a shear layer to a periodically oscillating point force from a series of wave packets. Our main tool is a Duhamel-type superposition integral of the form

$$V(x, y, z, t) = \mathrm{e}^{+\mathrm{i}\omega_* t}\int_0^t v(x, y, z, \tau)\,\mathrm{e}^{-\mathrm{i}\omega_*\tau}\,\mathrm{d}\tau, \tag{23}$$

where $V(x, y, z, t)$ is the transverse velocity component associated with the harmonic problem generated by a volume force of the form $\boldsymbol{F} = (0, F_y, 0)$, where $F_y = -\epsilon\delta(x)\,\delta(y-y_0)\,\delta(z)\exp(\mathrm{i}\omega_* t)$. Here, ω_* is the (real) radian frequency of oscillation and $v(x, y, z, t)$ is the solution to the pulse problem. As mentioned in the §1, we shall treat the harmonic problem without introducing a Laplace transform in time. We do this in order to avoid the evaluation of a tricky contour integral in complex frequency space.

As shown by the author (Balsa 1988), it is possible to obtain $V(x, y, z, t)$ for large values of (x, z) by using, not the complete pulse solution for $v(x, y, z, t)$, but only its asymptotic form – namely, the wave packet. After substituting (21a) into (23), we find

$$\Delta U V(x, 1, z, t)\,\mathrm{e}^{-\mathrm{i}\omega_* t} = \int^{\Delta U t} \mathscr{H}\exp\left[T(h_0 - \mathrm{i}\omega_*/\Delta U)\right]\frac{\mathrm{d}T}{T} + \mathrm{CC}(\omega_*), \tag{24}$$

where CC(ω_*) denotes the complex conjugate of all the terms on the right-hand side of an equation provided that we first replace ω_* by $(-\omega_*)$. The integral in (24) is taken over the wave packet which is contained in the cone of influence (figure 3).

Note that the 'rapid phase' h (see (17a)) may be written as

$$h = \mathrm{i}\kappa\frac{G-U_m}{\Delta U}\cos\theta + \mathrm{i}\kappa\frac{L}{\Delta U}\sin\theta + \lambda(\kappa)\cos\theta, \tag{25}$$

so that $h = h[\kappa,\ \theta;\ (G-U_m)/\Delta U,\ L/\Delta U]$, $\kappa_0 = \kappa_0[(G-U_m)/\Delta U,\ L/\Delta U]$, and $\theta_0 = \theta_0[(G-U_m)/\Delta U, L/\Delta U]$. In equation (24), $h_0 = h[\kappa_0, \theta_0; x/T-U_m/\Delta U, z/T]$, where in the last equation κ_0 and θ_0 are evaluated at $(x/T-U_m/\Delta U)$ and (z/T). Of course, h_0, as expressed above, is exactly the same function as that given by (21b), although the third and fourth arguments have been changed. We shall always point out the functional form with which we are dealing. In this section, the arguments of h are given by (25).

As long as the instability is convective (see Huerre & Monkewitz 1985; Balsa 1988), that is, the positive t-axis is *not* contained in the cone of influence, the principal contribution to the integrals in (24) comes from a saddle point in T-space. Note that (24) is evaluated by analytic continuation into complex T-space. It is convenient to introduce a new variable of integration, ξ, defined by

$$T = \frac{x}{\xi + U_m/\Delta U}, \tag{26a}$$

so that the exponents in (24) become

$$x\frac{H_0(\xi) \mp \mathrm{i}\omega_*/\Delta U}{\xi + U_m/\Delta U}, \tag{26b}$$

where the upper and lower signs go with the first and second terms. In the rest of this paper, we restrict our attention to the evaluation of the first integral – similar results may be obtained for the second integral of (24). This is because frequencies ω_* and $(-\omega_*)$ have the same effect on the shear layer. Note that in view of (26a).

$$H_0(\xi) = h(\kappa_0, \theta_0; \xi, \eta), \tag{26c}$$

where

$$\eta = \eta(\xi) = (\xi + U_m/\Delta U)\, z/x, \tag{26d}$$

and κ_0 and θ_0 are evaluated at ξ and η.

The saddle point in complex ξ-space occurs at the point ξ_- where

$$\mathrm{i}\omega_* - \cos[\theta_0(\xi_-, \eta_-)]\,\omega[\kappa_0(\xi_-, \eta_-)] = 0, \tag{27}$$

and $\eta_- = \eta(\xi_-)$. $\omega = \omega(\kappa) = -\mathrm{i}\kappa U_m + \Delta U\lambda(\kappa)$ is the two-dimensional dispersion relation associated with the unstable Rayleigh mode. Actually, $\cos\theta_0\,\omega(\kappa_0)$ is precisely the three-dimensional dispersion relation as obtained from the Squire transformation. After using the standard results for the saddle point method as $x \to \infty$ (Dingle 1973, p. 135), we arrive at

$$V(x,\ 1,\ z,\ t)\,\mathrm{e}^{-\mathrm{i}\omega_* t} = (2\pi)^{\frac{1}{2}}\mathrm{i}\left(\frac{\cos\phi}{r}\right)^{\frac{1}{2}}\frac{\exp[\mathrm{i}\kappa_0 r\cos(\theta_0-\phi)]}{\Delta U(\xi+U_m/\Delta U)^{\frac{1}{2}}}$$
$$\times\frac{\mathscr{F}_1(\kappa_0)\,\kappa_0}{\{h_{\theta\theta}\cos^2 + 2\kappa_0 h_{\kappa\theta}\cos\cdot\sin + \kappa_0^2 h_{\kappa\kappa}\sin^2\}^{\frac{1}{2}}} + \text{second term}, \tag{28a}$$

where

$$x = r\cos\phi, \quad z = r\sin\phi, \tag{28b}$$

and all the quantities in the first term on the right-hand side of (28a) are evaluated at the saddle point $\xi = \xi_-$. For example, $\kappa_0 = \kappa_0(\xi_-, \eta_-)$, $\theta_0 = \theta_0(\xi_-, \eta_-)$, etc. Double subscripted variables denote partial differentiation (e.g. $h_{\theta\theta} = \partial^2 h/\partial\theta^2$) and the arguments of the trigonometric functions cos and sin in the curly brackets of (28a) are $(\theta_0 - \phi)$.

Equation (28a) is one of the principal results of this paper and will be fully discussed in the next section. At this point, however, we wish to make several preliminary observations. First, for a given base velocity distribution, the saddle point ξ_- depends on only a single parameter, namely, $z/x = \tan\phi$. Therefore, along different rays in (x, z)-space we will observe different complex wavenumbers (κ, θ) or (k, l), but we will find a fixed wavenumber along a given ray. This is an especially interesting result since an individual wave packet does not have this property. Because of this, (28a) looks very much like a spatial instability mode – the magnitude of the disturbance grows exponentially with distance $r = (x^2+z^2)^{\frac{1}{2}}$ along each ray. The disturbance velocity also has an intrinsic directionality and cylindrical spreading contained in the factor $(\cos\phi/r)^{\frac{1}{2}}$. This is due to the fact that propagation space has two space dimensions. The receptivity of the shear layer to periodic disturbances is contained in the function $\mathscr{F}_1[\kappa_0(\xi_-, \eta_-)]$, as explained in §3.

5. Discussion of results and conclusions

Before we discuss some of the intricacies of three-dimensional wave packets, it is desirable to take a quick look at one of them. In figure 4(a) we show the transverse velocity component at the upper edge of the shear layer [i.e. $v(x, 1, z, t)$] for $T = \Delta U t = 40$. The point force is located on the centre of the layer ($y_0 = 0$) and $U_1 = 1$, $U_2 = 0$. The strength of the impulse is arbitrarily chosen as $\epsilon = 2.5$.

In this figure, we see the kind of spatial structure which had been anticipated at the end of §3. In the streamwise direction, x, we observe several waves whose crests and troughs decay rather rapidly (within about one wavelength) on either side of the x-axis. The highest amplitude of the waves corresponds roughly to the centre of the packet. The entire pattern drifts downstream at the shear layer average velocity, U_m, while at the same time, more waves develop in the packet. This is because the physical (i.e. real part of the) wavenumber is nearly a constant along the x-axis (see figure 2; h_{0_1} is linear in x) while the overall size of the packet grows in proportion to time.

It is quite remarkable to observe that the wavefronts are almost perfectly parallel to the spanwise direction, z. This result is especially surprising in view of the well-known snapshots of wave packets in a wall boundary layer by Gaster (1975). One of Gaster's pictures is also shown in figure 4 for comparison. A striking feature of wave packets in boundary layers is the highly curved wavefronts. Roughly speaking, disturbances in shear layers are more 'two dimensional' than in boundary layers.

In a shear layer, wavefronts are straight because the base flow is antisymmetric about the mean velocity U_m. The last remark is certainly true for our piecewise linear profile, as well as for the so-called tanh family of profiles ($U = U_m + \Delta U/2 \tanh y$). The reason is that the Doppler-shifted frequency h_{0_1} is antisymmetric with respect to the z-axis so that $h_{0_1} \equiv 0$ in the spanwise direction for $x = U_m t$. Therefore, no oscillations are possible in the z-direction since the spanwise wavenumber is $\partial h_{0_1}/\partial z = 0$. Clearly, such antisymmetry does not hold in a wall boundary layer so that, in general, there will be significant oscillations in the spanwise direction. These oscillations result in a curved wavefront.

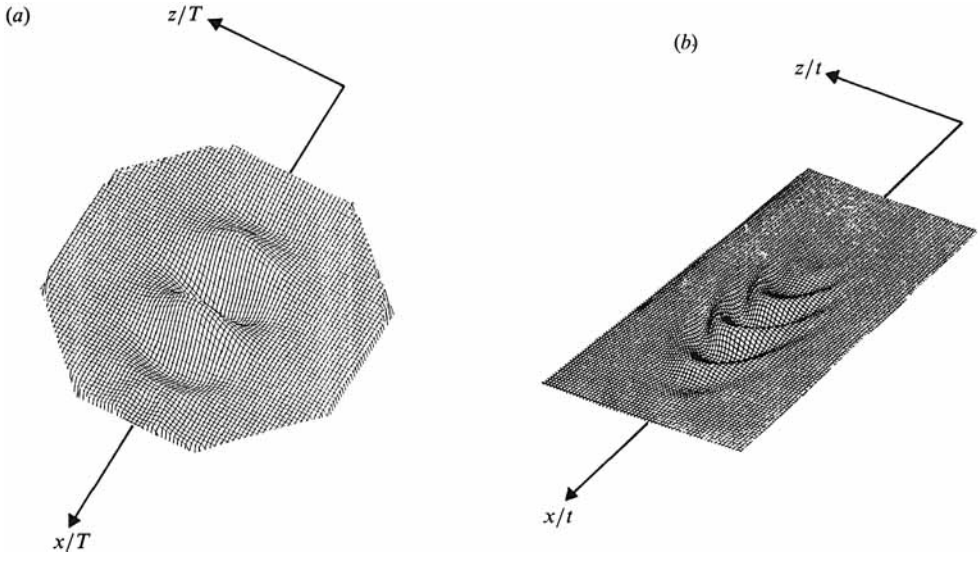

FIGURE 4. Qualitative comparison of wave packets in (*a*) free shear layer and (*b*) boundary layer (Gaster, 1975).

It is also enlightening to discuss briefly the location of the saddle points (κ_0, θ_0) in (κ, θ)-space. At the centre of the packet, $\kappa_0 = k_{\max}$ and $\theta_0 = 0$, where $k_{\max}$ is the real wavenumber associated with the maximum growth rate of two-dimensional *temporal* stability (for the piecewise linear and tanh profiles with $U_1 = 1$, $U_2 = 0$, $k_{\max}$ is 0.3984 and 0.4446, respectively). Indeed, the centre of the packet grows at the maximum growth rate of temporal stability. As we move away from the centre in the downstream direction ($\alpha = 0$), κ_0 moves into the upper half of the complex plane, more or less along a line parallel to the imaginary axis and passing through $\kappa = k_{\max}$. The value of θ_0 remains unchanged (i.e. $\theta_0 \equiv 0$). It is for this reason that a three-dimensional wave packet has exactly the same growth rate and frequency in the downstream direction as a two-dimensional one – the spanwise wavenumber $l = \kappa_0 \sin\theta_0 = 0$.

On the other hand, as we move away from the centre of the packet in the spanwise direction ($\alpha = \frac{1}{2}\pi$), κ_0 moves from $k_{\max}$ to the origin along the real axis and θ_0 is pure imaginary (though not a constant). In other words, in the spanwise direction the wave packet is comprised of instability modes whose streamwise and spanwise wavenumbers are $k = \kappa_0 \cos\theta_0 = \kappa_0 \cosh\theta_0^*$ and $l = \kappa_0 \sin\theta_0 = \mathrm{i}\kappa_0 \sinh\theta_0^*$ and θ_0^* is real. The spanwise wavenumber is purely imaginary! For other directions (i.e. for other values of α), κ_0 and θ_0 assume values that lie between the above two limiting cases.

We next turn to a brief discussion of wave packet similitude. The point of stationary phase (κ_0, θ_0) depends only on the non-dimensional variables $(\mathscr{V}/\Delta U, \alpha)$, which specify a (non-dimensional) point in the packet via (22). At such points, wave packets in different external streams will be identical, provided that the stretched variable $T = \Delta U t$ is used to measure time (see (21*a*)). This powerful similarity rule enables us to study wave packets in the canonical flow $U_1 = 1$, $U_2 = 0$ and, from these results, deduce the form of the packet in any other external stream. In this respect wave packets, which of course develop both in space and time, differ dramatically from spatial instability modes, for which the above similarity rule does not hold.

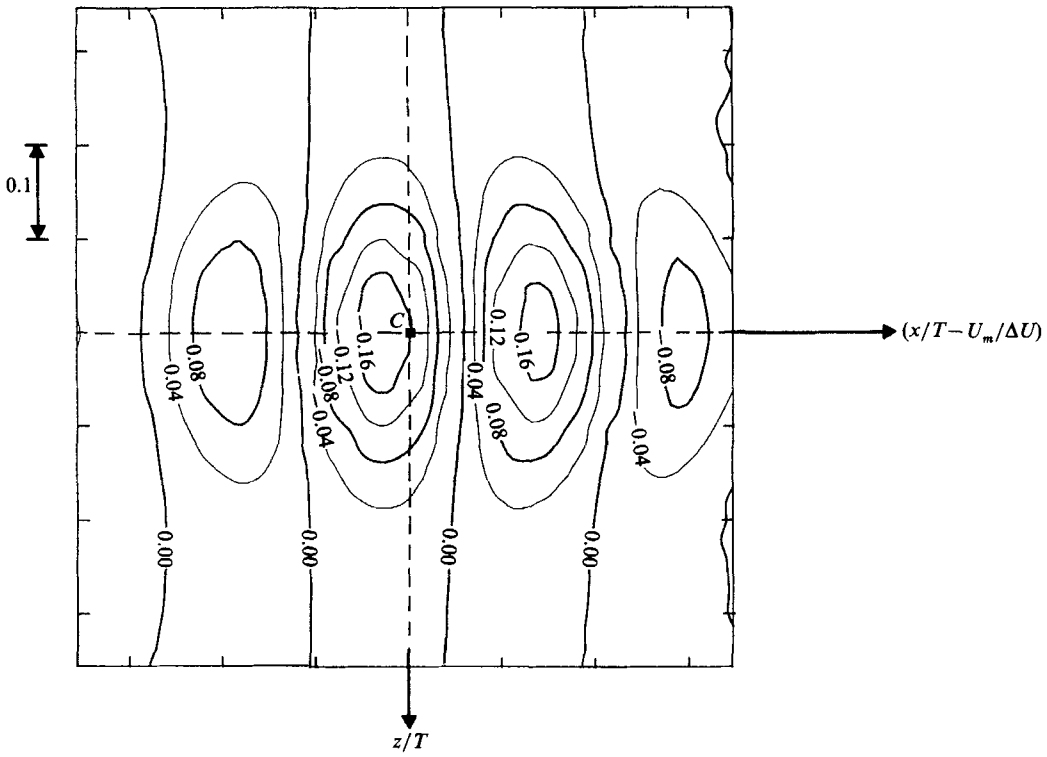

FIGURE 5. Contour map of wave packet (a) in figure 4 ($U_1 = 1$, $U_2 = 0$, $y_0 = 0$, $T = \Delta U t = 40$, $\epsilon = 2.5$).

Putting these remarks another way, the non-dimensional (inviscid) dynamics of a wave packet cannot be changed by altering the velocity ratio (U_1/U_2) across the shear layer.

We next come to the symmetry properties of the wave packet. The growth rate, h_{0_R}, and Doppler-shifted frequency, h_{0_I}, have certain symmetries that are not shared by the disturbance velocity $v(x, y, z, t)$. There is, trivially, left-to-right symmetry (facing downstream), but the upstream and downstream symmetries are lost. This is because of the presence of $\mathscr{H}$ in (21a) which also depends on x and z. The contour plot of our wave packet of figure 4(a) is shown in figure 5. The centre of the packet ($x = U_m t$, $z = 0$) is denoted by C. It is clear that the packet is not symmetric about the z-axis; very loosely speaking, there are generally 'more waves downstream than are upstream of the centre.' Observe that the planform of the packet is somewhat elliptical, with the major axis pointing in the direction of the base flow. (Note that the wiggles on the contours are caused by the plotting software.)

In figure 6, we show the evolution of the wave packet of figure 4(a) as a function of time. As time increases, more waves develop in the packet, and the peak amplitude of the wave increases in accordance with linear stability theory.

In figure 7, we show the behaviour of $v(x, 1, z, t)$ as a function of source location. As the force is moved from the centreline, $y_0 = 0$, the amplitude of the packet decreases. Hence, a shear layer is most sensitive or receptive to disturbances that are near its centre (i.e. the point about which the mean velocity profile is antisymmetric). Previously, such sensitivity has been explained in terms of 'critical layers', but the present analysis shows that such an explanation cannot be entirely correct since our

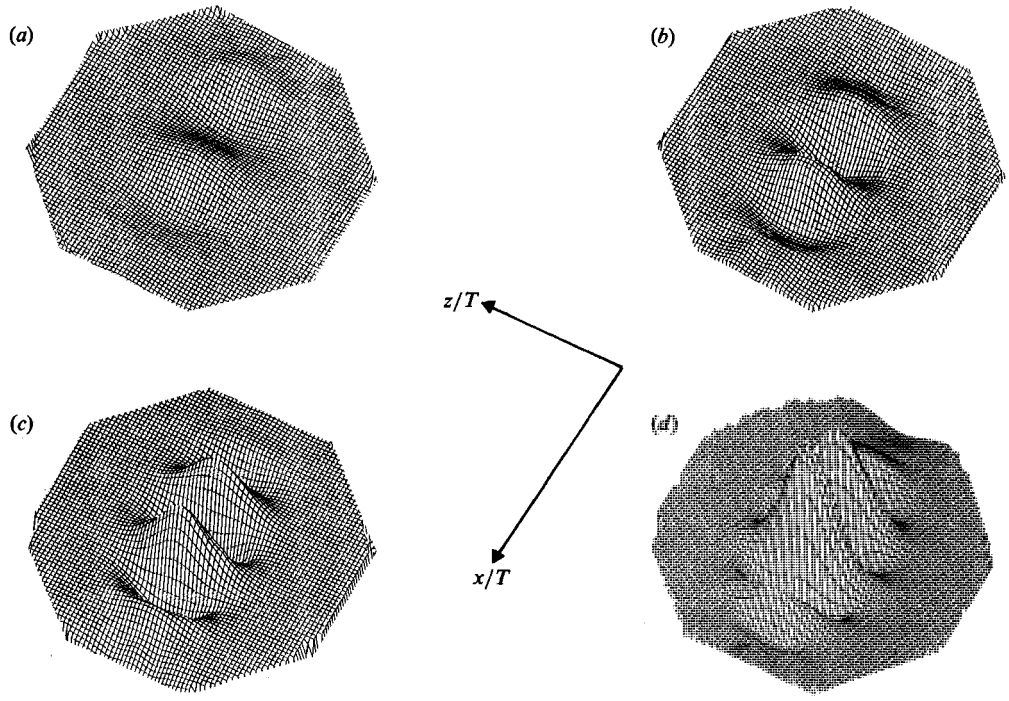

FIGURE 6. Evolution of a wave packet in: (*a*) time $T = \Delta Ut = 30$; (*b*) time $T = \Delta Ut = 40$; (*c*) time $T = \Delta Ut = 50$; and (*d*) time $T = \Delta Ut = 60$ ($U_1 = 1$, $U_2 = 0$, $y_0 = 0$, $\epsilon = 2.5$).

base velocity profile has no critical layer. A force near the upper interface of the shear layer (figure 7*c*) produces a larger velocity fluctuation at $y = 1$ than a force located near the lower edge of the layer. These remarks are easy to accept on simple physical grounds.

We next discuss the results for the excitation of a shear layer, with external streams $U_1 = 1.5$, $U_2 = 0.5$, by a periodically oscillating point force of radian frequency ω_*. Since (28*a*) is the first term of an asymptotic expansion for large values of r, this result is valid as long as the spatial growth rate $\sigma > 0$, where

$$\sigma = \mathrm{Re}\,[i\kappa_0 \cos(\theta_0 - \phi)], \tag{29}$$

$\kappa_0 = \kappa_0(\xi_-, \eta_-)$, and $\theta_0 = \theta_0(\xi_-, \eta_-)$. Otherwise, our leading term is exponentially small, therefore, it cannot be the correct first term of our asymptotic series.

In figure 8, we show the half-wedge angle $\phi_{\max}$ as a function of excitation frequency ω_*. As long as $-\phi_{\max} < \phi < \phi_{\max}$ (recall $x = r\cos\phi$, $z = r\sin\phi$), the spatial growth rate, σ, is positive and, in this wedge of (x, z)-space, we have a three-dimensional spatial instability wave. Outside this wedge, disturbances are exponentially small in a relative sense. At low frequencies, the half-wedge angle is about 26.6°, and it decreases with increasing frequency, ω_*. Roughly speaking, high-frequency disturbances are beamed along the downstream direction. Near-neutral waves can grow exponentially only in a slender wedge in the vicinity of the x-axis. It is interesting to speculate how a three-dimensional instability wave of this type would be focused down to the x-axis in a slowly diverging base flow.

We next develop an asymptotic theory for the half-wedge angle $\phi_{\max}$ at low frequencies. This is simple to do if we think of a spatial mode as a superposition of

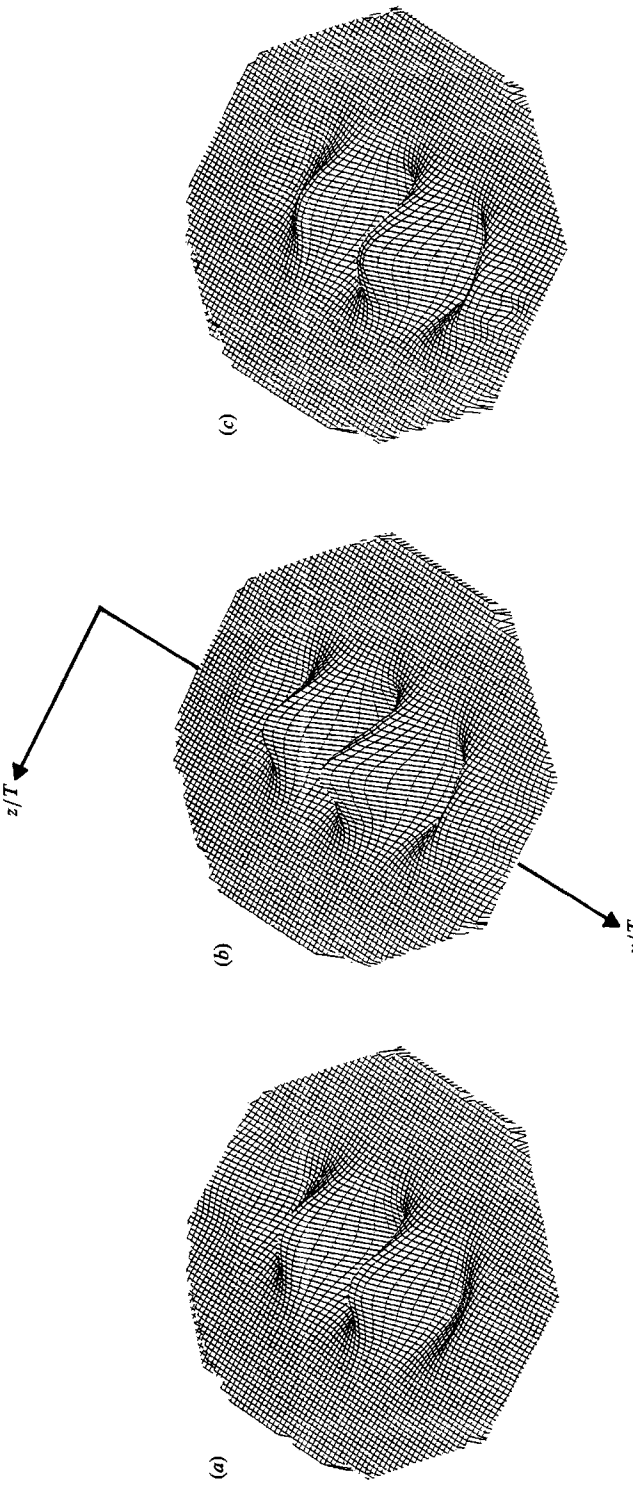

FIGURE 7. Receptivity of a shear layer to pulse-type input: (*a*) $y_0 = -0.7$; (*b*) $y_0 = 0$; (*c*) $y_0 = +0.7$ ($T = \Delta Ut = 40$, $U_1 = 1$, $U_2 = 0$, $\epsilon = 2.5$).

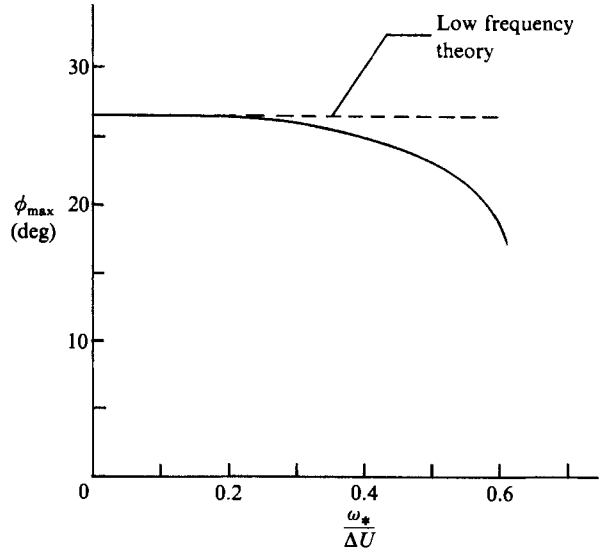

FIGURE 8. Semi-wedge angle of an instability wave as a function of excitation frequency ($U_m/\Delta U = 1$).

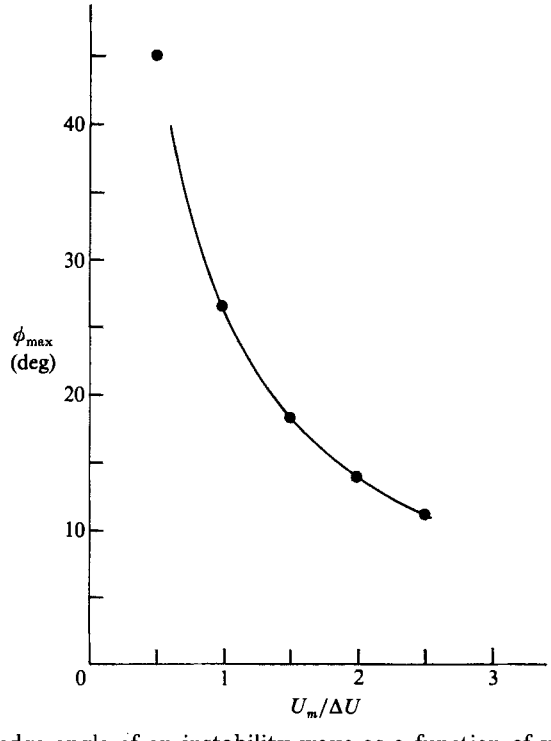

FIGURE 9. Semi-wedge angle of an instability wave as a function of velocity ratio ($\omega_*/\Delta U$ 0.3): —, numerical results; ●, low-frequency theory.

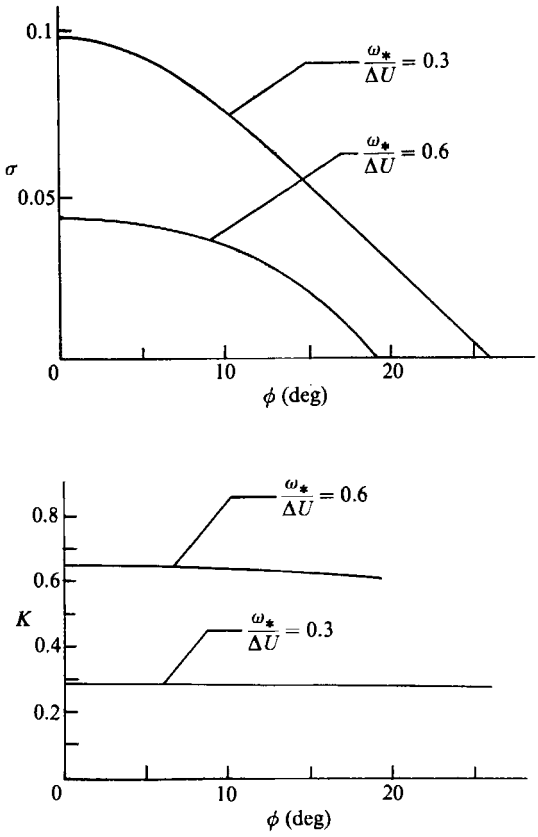

FIGURE 10. Growth rate and wavenumber of an instability wave as a function of polar angle $(U_m/\Delta U = 1)$.

wave packets. A wave packet, emitted at $t = 0$, has its centre at $x = U_m t$ at time t, and its 'radius' is approximately $0.5\,\Delta U t$. Therefore, there is 'no' disturbance outside the wedge with semi-vertex angle $\tan^{-1}(0.5\,\Delta U/U_m)$. Wave packets that are emitted by the oscillating source at later instants of time simply fill the interior of this wedge. Apparently, this result overestimates the actual wedge angle at high frequencies (figure 8). This is due to the fact that there is cancellation at high frequencies near the boundary of the wedge since the growth rates are small and the waves can destructively interfere.

The similitude of our spatial instability mode can be expressed in terms of similarity parameters $(\omega_*/\Delta U)$ and $(U_m/\Delta U)$. In figure 9, we show the dependence of the wedge angle, $\phi_{\max}$, on $(U_m/\Delta U)$ at a fixed value of $\omega_*/\Delta U = 0.3$ (low frequency). The solid line represents the exact results obtained numerically, and the dots represent our low-frequency theory. There is excellent agreement between the two sets of results. Note that our three-dimensional instability wave can be made as slender as we please by increasing the mean velocity, U_m, with respect to the velocity difference, ΔU. This is analogous to increasing the flow velocity with respect to the speed of sound in supersonic flows.

In figure 10, we show the spatial growth rate, σ, and the wavenumber, K, where

$$K = \mathcal{I}m[\mathrm{i}\kappa_0 \cos(\theta_0 - \phi)], \tag{30}$$

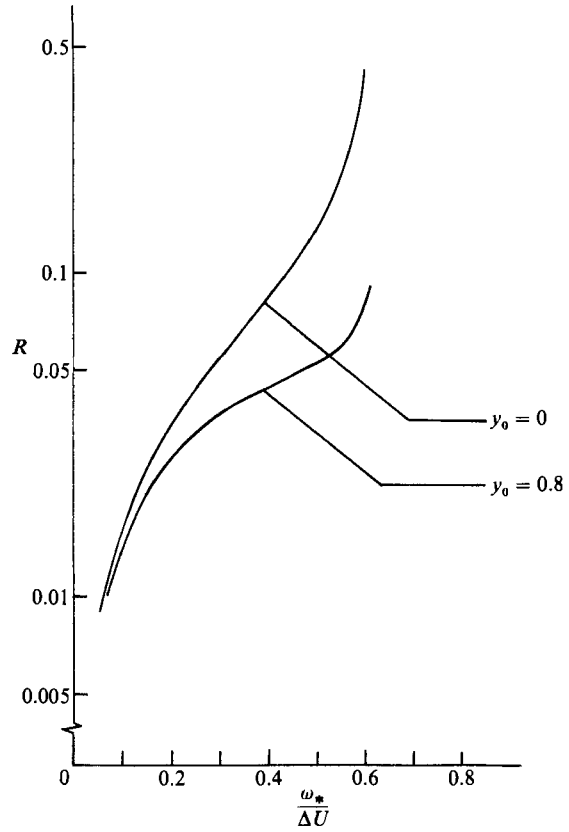

FIGURE 11. Receptivity as a function of excitation frequency and source location ($U_m/\Delta U = 1$, $\epsilon = 1$, $r = 1$, $\phi = 0$).

as a function of polar angle ϕ. The wavenumber is roughly proportional to the excitation frequency, and its variation with ϕ is very small. Therefore, the wavefronts of our three-dimensional instability waves are slightly curved. On the other hand, the growth rates depend strongly on the polar angle ϕ. As in the case of the wave packet, the maximum growth rate occurs along the downstream direction. The point where $\sigma = 0$ defines the edge of the instability wave at each frequency. This has already been discussed in terms of our wedge angle $\phi_{\max}$.

The receptivity of the shear layer to three-dimensional periodic disturbances may be measured by

$$R = \left|(2\pi)^{\frac{1}{2}}\left(\frac{\cos\phi}{r}\right)^{\frac{1}{2}} \frac{1}{(\xi + U_m/\Delta U)^{\frac{1}{2}}\{h_{\theta\theta}\cos^2 + 2\kappa_0 h_{\kappa\theta}\cos\cdot\sin + \kappa_0^2 h_{\kappa\kappa}\sin^2\}^{\frac{1}{2}}} \frac{\mathscr{F}_1(\kappa_0)\,\kappa_0}{}\right|, \tag{31}$$

evaluated at the saddle point ξ_-. Equation (31) essentially comes from the solution for the transverse velocity component (see (28*a*)), and we may think of R as the 'amplitude' of our three-dimensional spatial instability mode whose value is determined by the location of the force (y_0), its frequency (ω_*), and the external stream velocities (U_1 and U_2).

We show the dependence of R on excitation frequency ω_* and force location y_0 in figure 11. We see that the receptivity of the shear layer increases monotonically by

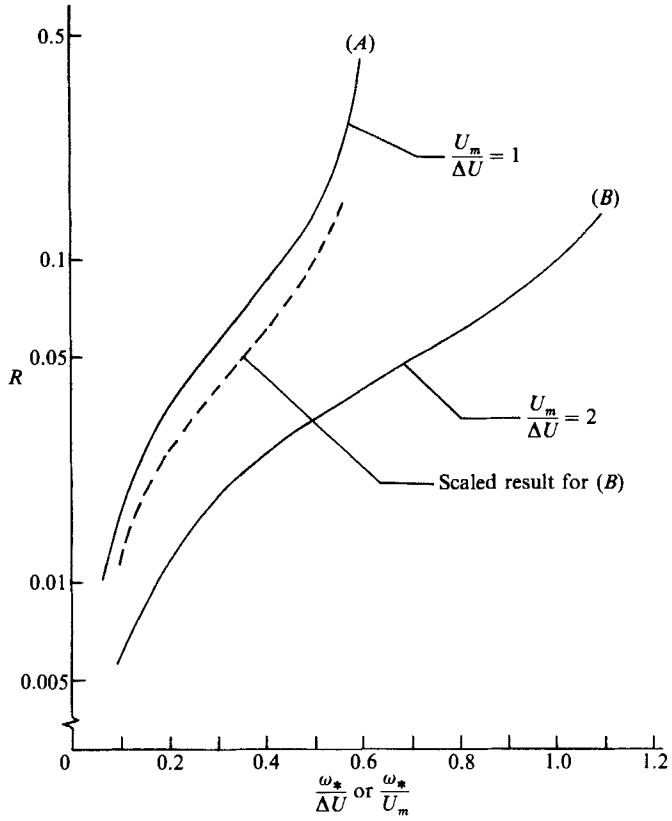

FIGURE 12. Receptivity as a function of frequency and external stream velocities; horizontal axis $\omega_*/\Delta U$ applies to curves A and B and ω_*/U_m applies to curves A and rescaled B ($y_0 = 0$, $\epsilon = 1$, $r = 1$, $\phi = 0$).

about one order of magnitude (for $y_0 = 0$) as the frequency is increased over the range of interest. As the force is moved from the centreline toward the upper edge of the shear layer, the receptivity decreases, especially at higher frequencies. At low frequencies, of course, one expects negligible change. It is quite remarkable that a shear layer has such strong intrinsic receptivity to disturbances of various frequencies. In order to elicit the strongest response, the disturbance should be placed on the shear layer centreline. These remarks are completely consistent with our observations on the wave packet and two-dimensional waves (Balsa 1988). As the excitation frequency is further increased and approaches the neutral frequency, the receptivity becomes very large. We believe this is an unphysical result which has its origin in the branch cut singularity of the dispersion relation (Balsa 1987).

Finally, we compare the receptivities of two shear layers with different external streams when the force is on the shear layer centreline (figure 12). The large difference between the two solid curves A and B can be considerably reduced by treating $(\omega_*/\mathrm{U_m})$ (rather than $\omega_*/\Delta U$) as one of our similarity variables. This rescaling of curve B results in the dashed curve. We conclude that the receptivity of the shear layer depends quite strongly on $(\omega_*/\mathrm{U_m})$ but rather weakly on $(U_m/\Delta U)$.

The author wishes to express his gratitude to NASA Lewis Research Center for financial support under grant NAG 3-485.

REFERENCES

BALSA, T. F. 1987 On the spatial instability of piecewise linear free shear layers. *J. Fluid Mech.* **174**, 553–563.

BALSA, T. F. 1988 On the receptivity of free shear layers to two-dimensional external excitation. *J. Fluid Mech.* **187**, 155–177.

BAYLY, B. J. 1986 Three-dimensional instability of elliptical flow. *Phys. Rev. Lett.* **57**, 2160–2163.

BETCHOV, R. & CRIMINALE, W. O. 1967 *Stability of Parallel Flows*. Academic.

CASE, K. M. 1960 Stability of inviscid plane Couette flow. *Phys. Fluids* **3**, 143–148.

CASE, K. M. 1961 Hydrodynamic stability and the inviscid limit. *J. Fluid Mech.* **10**, 420–429.

CRAIK, A. D. D. & CRIMINALE, W. O. 1986 Evolution of wavelike disturbances in shear flows: a class of exact solutions of the Navier–Stokes equations. *Proc. R. Soc. Lond.* A **406**, 13–26.

CRIGHTON, D. & GASTER, M. 1976 Stability of slowly diverging jet flow. *J. Fluid Mech.* **77**, 397–413.

CRIMINALE, W. O. & KOVASZNAY, L. 1962 The growth of localized disturbances in a laminar boundary layer. *J. Fluid Mech.* **12**, 59–80.

DINGLE, R. B. 1973 *Asymptotic Expansions: Their Derivation and Interpretation*. Academic.

DRAZIN, P. G. & REID, W. H. 1981 *Hydrodynamic Stability*. Cambridge University Press.

GASTER, M. 1968 The development of three-dimensional wave packets in a boundary layer. *J. Fluid Mech.* **32**, 173–184.

GASTER, M. 1975 A theoretical model of a wave packet in the boundary layer on a flat plate. *Proc. R. Soc. Lond.* A **347**, 271–289.

GASTER, M. 1981 Propagation of linear wave packets in laminar boundary layers. *AIAA J.* **19**, 419–423.

GASTER, M. & DAVEY, A. 1968 The development of three-dimensional wave packets in unbounded parallel flows. *J. Fluid Mech.* **32**, 801–808.

GASTER, M., KIT, E. & WYGNANSKI, I. 1985 Large-scale structures in forced turbulent mixing layer. *J. Fluid Mech.* **150**, 23–39.

GOLDSTEIN, M. E. 1983 The evolution of Tollmien–Schlichting waves near a leading edge. *J. Fluid Mech.* **127**, 59–81.

GOLDSTEIN, M. E. & LEIB, S. J. 1988 Nonlinear roll-up of externally excited free shear layers. *J. Fluid Mech.* **191**, 481–515.

HAYES, W. D. 1970 Conservation of action and modal wave action. *Proc. R. Soc. Lond.* A**320**, 187–208.

HUERRE, P. & MONKEWITZ, P. 1985 Absolute and convective instabilities in free shear layers. *J. Fluid Mech.* **159**, 151–168.

LAGNADO, R. R., PHAN-THIEN, N. & LEAL, L. G. 1984 The stability of two-dimensional linear flows. *Phys. Fluids* **27**, 1094–1101.

MICHALKE, A. 1969 A note on spatially growing three-dimensional disturbances in a free shear layer. *J. Fluid Mech.* **38**, 765–767.

MONKEWITZ, P. A. & NGUYEN, L. N. 1987 Absolute instability in the near-wake of two-dimensional bluff bodies. *J. Fluids Struct.* **1**, 165–184.